The Society of Naval Architects of Japan

Numerical Study of Vortical Flows beneath the Free Surface around Struts

Uh-Cheul Jeong*, *Member* Yasuaki Doi**, *Member*

Summary

Characteristics of vortical flows around free surface piercing struts are studied by a numerical simulation method solving 3-D laminar incompressible Navier-Stokes and continuity equations. The simulation shows that vorticity is generated on the curved free surface to satisfy a no-shearing stress condition. The vorticity, whose strength is proportional to the free surface curvature, leads the generation of the vortical motions beneath the free surface in front of a bow. To investigate curvature effect of the body, three different struts having NACA 0005, NACA 0008 and NACA 0012 sections are used. The effect of free surface boundary conditions and grid density around the free surface are also discussed.

1. Introduction

Bow wave breaking is one of the most noticeable phenomena in the field of ship hydrodynamics. Since Baba[1] and Taneda et al.[2] independently pointed out its importance, many investigations have been made to clarify the mechanism of the breaking waves.

Kayo et al.[3] carried out a flow visualization test around a bow. They explained that a shear flow might exist on the free surface and the shear flow had a significant effect on the formation of the bow breaking waves and vortical motions. Takekuma et al.[4] made a simillar conclusion and they reported that the intensity of the vortical motions around the body with a shallower draft was larger than that with a deeper draft. Experimental observation for this draft effect was also carried out by Ogiwara et al.[5] and they reported that the vortex motions were mainly generated by the flow above the stagnation point on the body surface. Miyata et al.[6] explained that overturning of waves generated a necklace vortex of which intensity depended on the strength of the overturning motion. They also reported that the vorticity generated by the breaking waves spreaded forward by the movement of wave front and backward by diffusive effect. However, Mori[7] deduced that the free surface curvature played a role to generate a vorticity on the free surface and the vorticity could be one of the sources of the necklace vortex. He investigated the curvature effect of the bow using a circular cylinder and an elliptic strut. According to his experimental results, the bow with a larger curvature (elliptic strut) generated more intensive wrinkle, which was a kind of free surface instability, than that generated by the bow with a smaller one (circular cylinder) at the same speed. Matsui et al.[8] also showed that the curvature of the vertical strut affected the bow breaking waves.

In this paper, the characteristics of the vorticity generated on the free surface around struts are studied by a numerical simulation method. In order to elucidate the effect of the vorticity and to exclude the effect of the draft, simulations are carried out for the struts having deep draft. The effect of a surface tension is neglected for the simplicity. To investigate the curvature effect of the bow, three different struts having NACA 0005, NACA 0008 and NACA 0012 sections are used. Some investigations concerning the effect of free surface boundary treatment and grid density around the free surface are carried out. The computed wave profiles are compared with experimental data.

2. Computational Method

2.1 Governing equations and numerical scheme

Three dimensional laminar incompressible Navier-Stokes (NS) and continuity equations are employed for the present numerical study. These governing equations are written as follows;

$$\frac{\partial u}{\partial t}+u\frac{\partial u}{\partial x}+v\frac{\partial u}{\partial y}+w\frac{\partial u}{\partial z}=-\frac{\partial \phi}{\partial x}+\frac{1}{Rn}\nabla^2 u$$

* Graduate school, Hiroshima University
** Hiroshima University

Received 10th July 1995
Read at the Autumn meeting 16, 17th Nov. 1995

NII-Electronic Library Service

The Society of Naval Architects of Japan

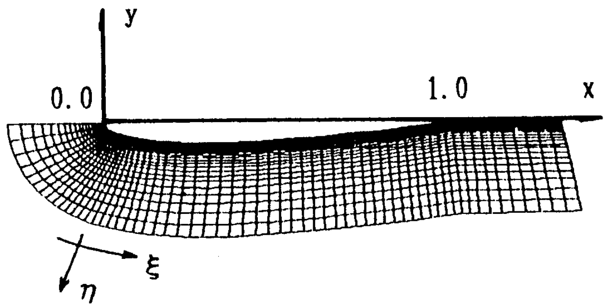

Fig. 1 Co-ordinate systems and generated grid near body at horizontal plane; NS12.

$$\frac{\partial v}{\partial t}+u\frac{\partial v}{\partial x}+v\frac{\partial v}{\partial y}+w\frac{\partial v}{\partial z}=-\frac{\partial \phi}{\partial y}+\frac{1}{Rn}\nabla^2 v$$
$$\frac{\partial w}{\partial t}+u\frac{\partial w}{\partial x}+v\frac{\partial w}{\partial y}+w\frac{\partial w}{\partial z}=-\frac{\partial \phi}{\partial z}+\frac{1}{Rn}\nabla^2 w \qquad (1)$$
$$\phi=p+\frac{z}{Fn^2}-P_n$$

$$\frac{\partial u}{\partial x}+\frac{\partial v}{\partial y}+\frac{\partial w}{\partial z}=0 \qquad (2)$$

where, (u, v, w) are the velocity components in (x, y, z)-directions in the Cartesian co-ordinate system as shown in Fig. 1; x in the uniform flow, y in the lateral and z in the vertical directions respectively. The origin is located at the leading edge of the strut on the undisturbed free surface. ϕ, p, P_{at}, Fn and Rn are modified pressure, pressure, atmospheric pressure, Froude number and Reynolds number respectively. All the variables are nondimensionalized by a uniform velocity (Uo) and a length of the strut (L).

The basic concept of the solution algorithm is based on the MAC method. A finite difference method is represented on a regular grid system. So all the variables are defined on the grid nodes. The first order differencing of the time derivatives in NS equations is used for an explicit advencement in time. The convective terms in NS equations are descretized by the third order upwind scheme while the first order upwind scheme is used on the boundaries. All the other spatial derivatives are descretized by the second order central differencing scheme except the boundary points while oneside differencing scheme is introduced on the boundaries.

2.2 Grid generation

A numerical co-ordinate transformation is introduced into the body fitted co-ordinate system to simplify the computational domain and to facilitate the implementation of boundary conditions. C-H type grid is employed for the present computation. C-type grid is generated by using geometrical method[9] and the whole grid system is obtained by stacking them in the vertical direction algebraically. The grid topology near the body at a horizontal plane and the curvilinear co-ordinate system are shown in Fig. 1. The ζ-axis of the body fitted co-ordinate system coincides with the z-axis. The grid lines are clustered near the body and the free surface to simulate properly the free surface and viscous interaction.

3. Boundary Conditions

3.1 Free surface boundary conditions

A viscous free surface boundary condition can be represented by an equilibrium of stresses on the free surface as equation (3);

$$\sigma_{ij}\boldsymbol{n}_j=\sigma^*_{ij}\boldsymbol{n}_j \qquad (3)$$
$$\sigma_{ij}=-p\delta_{ij}+\frac{1}{Rn}\left(\frac{\partial u_i}{\partial x_j}+\frac{\partial u_j}{\partial x_i}\right)$$

where σ_{ij}, σ^*_{ij}, $\boldsymbol{n}_j$ and δ_{ij} are fluid stress tensor, external stress tensor, unit outward normal vector to the free surface and Kronecker delta respectively in the Cartesian co-ordinate system. Assuming no-surface tension and no-shearing stress, equation (3) can be rewritten as follow;

$$\sigma_{ij}\boldsymbol{n}_j\boldsymbol{n}_i=P_{at} \qquad (4)$$
$$\sigma_{ij}\boldsymbol{n}_j\boldsymbol{t}_i=0 \qquad (5)$$

where $\boldsymbol{t}_i$ is unit tangential vector to the free surface. Finally, the following equations can be used as a dynamic free surface boundary condition assuming that the viscous stress in the normal direction to the free surface can be zero.

$$\phi=\frac{h}{Fn^2} \qquad (6)$$

$$2\frac{\partial u}{\partial x}\boldsymbol{n}_x+\left(\frac{\partial u}{\partial y}+\frac{\partial v}{\partial x}\right)\boldsymbol{n}_y+\left(\frac{\partial u}{\partial z}+\frac{\partial w}{\partial x}\right)\boldsymbol{n}_z=0$$
$$\left(\frac{\partial u}{\partial y}+\frac{\partial v}{\partial x}\right)\boldsymbol{n}_x+2\frac{\partial v}{\partial y}\boldsymbol{n}_y+\left(\frac{\partial v}{\partial z}+\frac{\partial w}{\partial y}\right)\boldsymbol{n}_z=0 \qquad (7)$$
$$\left(\frac{\partial w}{\partial x}+\frac{\partial u}{\partial z}\right)\boldsymbol{n}_x+\left(\frac{\partial w}{\partial y}+\frac{\partial v}{\partial z}\right)\boldsymbol{n}_y+2\frac{\partial w}{\partial z}\boldsymbol{n}_z=0$$

where h, $\boldsymbol{n}_x$, $\boldsymbol{n}_y$ and $\boldsymbol{n}_z$ are wave height and (x, y, z)-components of the unit outward normal vector to the free surface respectively. Solving above simultaneous equations (equation (7)) on the free surface, the velocity components can be calculated.

The no-shearing stress condition leads a generation of the vorticity on the free surface[10]. The axis of the vorticity is perpendicular to the streamwise direction and the strengh of the vorticity is

$$\omega=2\boldsymbol{k}_s\boldsymbol{q}_s \qquad (8)$$

where, $\boldsymbol{k}_s$ and $\boldsymbol{q}_s$ are the curvature of stream line and streamwise velocity on the free surface respectively. Equation (8) means that the curvature of the free surface can generate the vorticity if the streamwise velocity is not zero.

A zero-gradient extrapolation for the velocity is commonly used on the free surface because of the simplicity. In the present computation, the above two approaches are compared together.

The free surface location can be calculated by satisfying the kinematic free surface boundary condition (equation (9)) which represents that the fluid particles of the free surface always remain on it. Equation (9) is descretized by the third order upwind scheme in the present study.

NII-Electronic Library Service

The Society of Naval Architects of Japan

$$\frac{\partial h}{\partial t}+u\frac{\partial h}{\partial x}+v\frac{\partial h}{\partial y}-w=0 \qquad (9)$$

3.2 Other boundary conditions

The uniform velocity and zero-wave elevation are used as an upstream boundary condition. A symmetry condition for all the variables related to velocity, pressure and wave height is imposed at the symmetric plane on the half-C domain. On the body surface, no-slip condition is imposed and the wave height is linearly extrapolated. As a deep draft is assumed in the present computations, the bottom of the strut corresponds to the bottom boundary. A zero-gradient extrapolation is used as a bottom boundary condition.

Sometimes, improper boundary conditions give some numerical troubles such as reflection or oscillation of waves on the outer boundaries[11]. However, a simple zero-gradient extrapolation can be acceptable to investigate the flow near the body because the outer boundary or the grid arrangement around the far field region does not affect so much the flow near the body when the computational domain is large enough. In the present computations, a simple zero-gradient extrapolation is used on all the outer boundaries.

4. Numerical Simulations and Discussions

4.1 Computational conditions

Several computations are performed for the three different struts having NACA 0005, NACA 0008 and NACA 0012 sections (called NS 05, NS 08 and NS 12 respectively hereafter). Computational domains are $-2.0 \leq x \leq 4.0$, $0.0 \leq y \leq 2.0$ and $-1.0 \leq z \leq h_{\max}$ for all the computational cases. Computational conditions for the standard cases are listed in Table 1. These standard conditions are chosen through various test computations. The results for a half of time increment and of minimum grid spacing give almost the same results with the standard cases.

In the present computations, the flow is accelerated from a rest condition to the uniform velocity. The flow acceleration may affect the bow wave formations. For instance, a sudden acceleration may lead strong oscillatory motion or overturning of wave around a bow. In order to avoid such a strong wave-breaking, the flow is slowly accelerated up to nondimensional time T=5.0 in the present computations. Fig. 2 shows one example of the time history of a bow wave elevation for NS 05 at Rn=5000 and Fn=0.30. The bow wave reaches to the steady state after the acceleration.

Table 1 Computational conditions for standard cases.

	Rn=5000	Rn=10000 and 40000
Grid numbers		
- ξ-direction	91	110
- η-direction	45	50
- ζ-direction	20	20
Min. grid spacings		
- $\Delta\xi$	0.005	0.005
- $\Delta\eta$	0.002	0.002
- $\Delta\zeta$	0.0015	0.001
Time increment	0.001	0.0005

4.2 Vortical motions around bows

Fig. 3 shows time evolutions of the bow wave formation at center plane during the acceleration for NS 05 at Rn=5000 and Fn=0.30. Schematic view of the bow wave at center plane is shown in Fig. 4. The "Zone-I" is the part ahead of the bow where the free surface has smooth concave curvature. Through a sharp change of the curvature, the flow enters "Zone-II" where the flow may not be stable. The "wave front" is a border of these two zones[7]. At T=3.0 in Fig. 3, counter-clockwise vorticity (dotted lines) falls appearing on the free surface which has concave curvature (Zone-I). The vorticity is generated on the free surface to satisfy the no-shearing stress condition (equation (8)). Increasing the upstream velocity, the curvature of the free surface and the strength of the vorticity increase together. Around T=4.0, a sharp change of the curvature appears obviously and the peak of the vorticity is located just beneath the free surface around there, however no significant reverse flow is observed. The flow reaches to the steady state gradually after the acceleration (T=5.0).

Fig. 5 shows the vorticity (ω_y) distributions on the free surface at center plane. Wave height (h) and the streamwise velocity (q_s) on the free surface are plotted together. The peaks of the vorticity are located on the free surface having concave curvature (Zone-I) as indicated by dotted arrows. According to the no-shearing stress condition (equation (8)), the vorticity on the free surface can be expressed as the product of the free surface curvature and the streamwise velocity. Although the wave front has a larger curvature than that of the concave surface (Zone-I), the vorticity is smaller at the wave front because the streamwise velocity becomes smaller around there. This is the reason why the counter-clockwise vorticity occupies the region in front of the bow.

The model with larger curvature (NS 05) intensifies the concave curvature of the free surface and generates stronger vorticity comparing with other models (NS 08

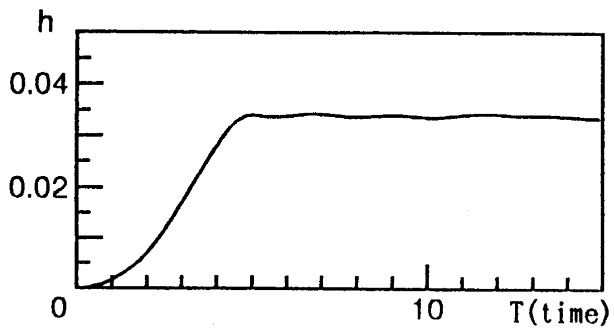

Fig. 2 Time history of bow wave elevation: NS12, Rn=5000, Fn=0.30.

NII-Electronic Library Service

The Society of Naval Architects of Japan

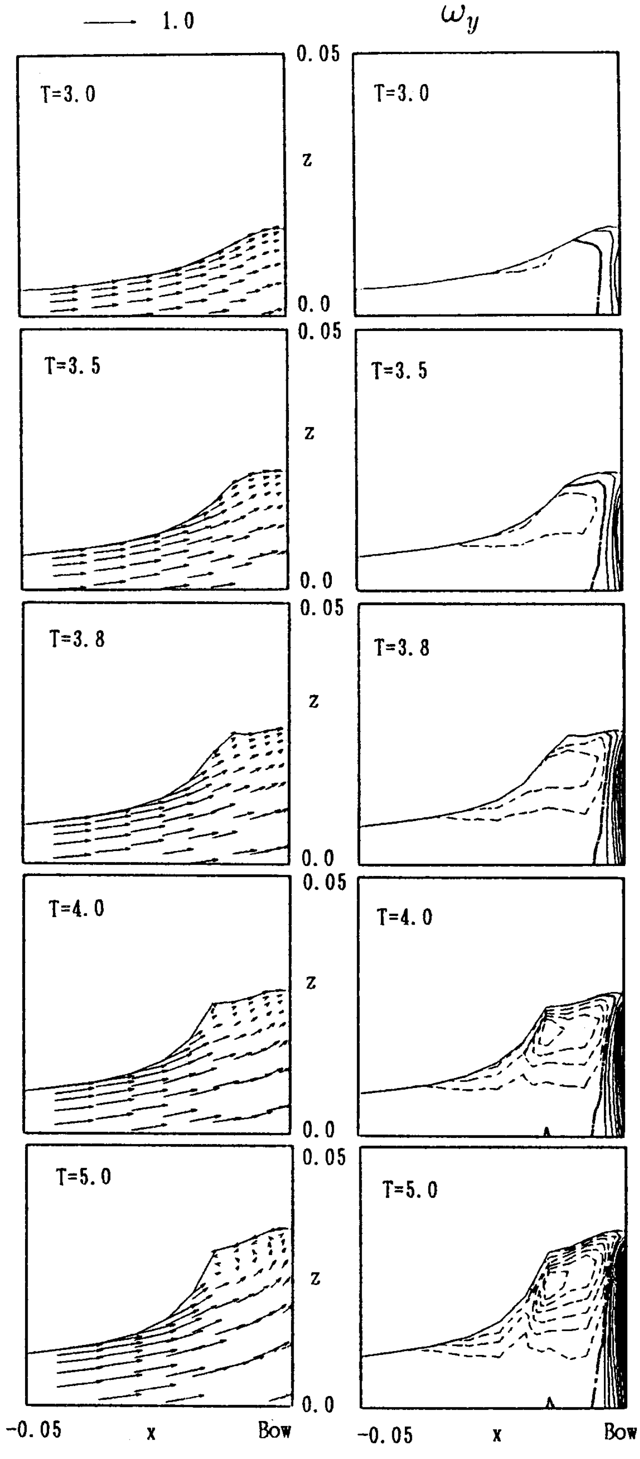

Fig. 3 Time evolutions of bow wave formation at center plane; NS05, Rn=5 000, Fn=0.30.
Left: velocity vectors.
Right: vorticity (ω_y) distributions (contour interval=10.0).

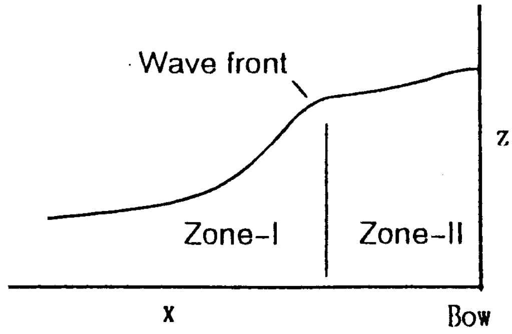

Fig. 4 Schematic view of bow wave.

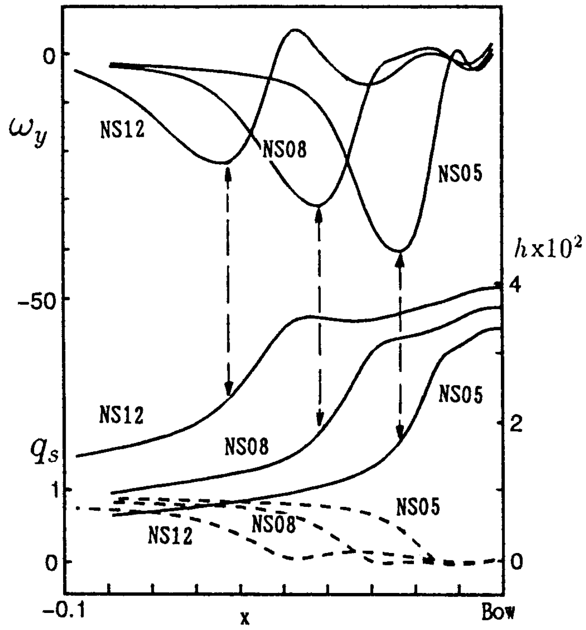

Fig. 5 Comparison of vorticity (ω_y), wave profile (h) and streamwise velocity (q_s) on the free surface at center plane, T=15.0.

and NS 12). This situation is cleary seen in Fig. 6 which shows the vorticity (ω_y) and velocity distributions at center plane in front of the bows of the three models. The model with larger curvature (NS 05) generates the most intensive vorticity. The peak of the vorticity is located beneath the free surface around the wave front for each struts.

Fig. 7 shows the velocity distributions on the free surface around the bows. The wave front line of NS 05 is clearly observed. Decreasing the curvarure of the bow, this line goes away from the body and becomes weak.

These results may give some explanations to the finding of Mori[7] who showed that the bow with a larger curvature (elliptic strut) generated more intensive wrinkle, which was a kind of free surface instability, than that generated by the bow with a smaller one (circular cylinder) at the same speed. He explained that the reason might be the different curvature of the free surface.

Figs. 8 and 9 show the vorticity distributions beneath the free surface around the bows. The distance from the free surface is about 0.005. The vorticity distributed

NII-Electronic Library Service

The Society of Naval Architects of Japan

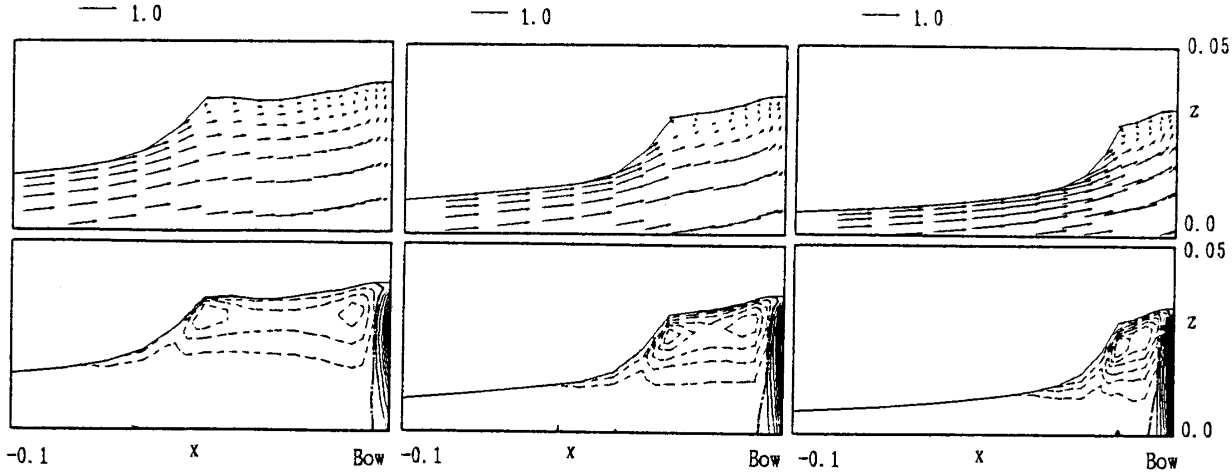

(a) NS12 (b) NS08 (c) NS05

Fig. 6 Computed velocity and vorticity (ω_y) distributions at center plane in front of bow: effect of bow curvature; NS05, NS08 and NS12, Rn=5000, Fn=0.30, T=15.0 (contour interval=10.0)

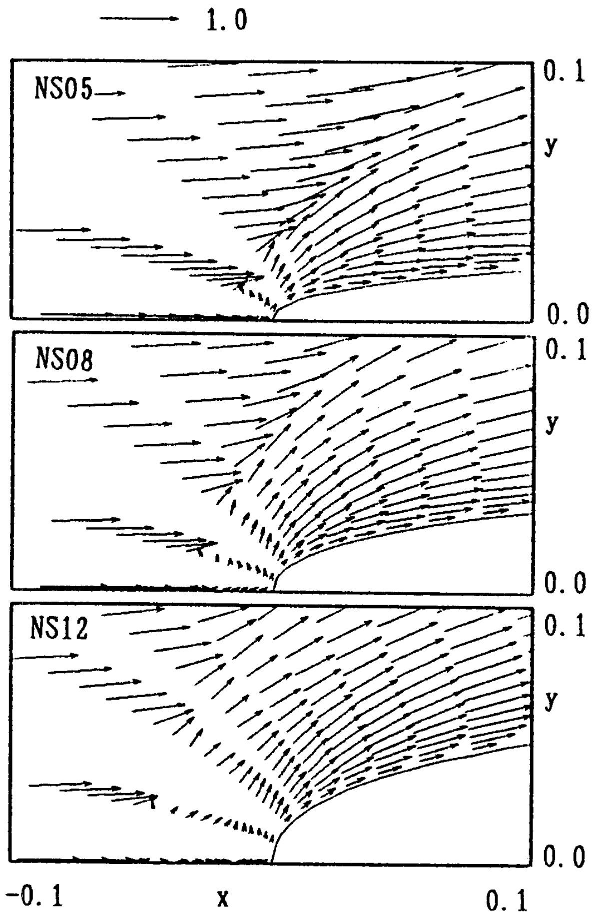

Fig. 7 Computed velocity vectors on the free surface for NS05, NS08 and NS12 from above, Rn=5000, Fn=0.30, T=15.0.

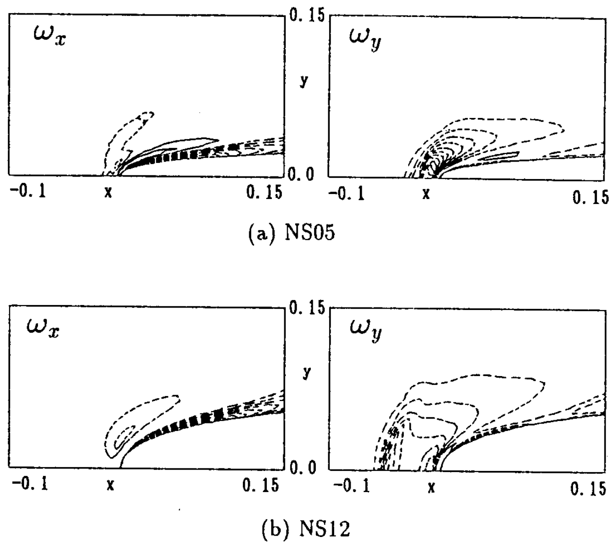

Fig. 8 Vorticities (ω_x, ω_y) distributions beneath the free surface; NS05 and NS12, Rn=5000, Fn=0.3, T=15.0 (contour interval=5.0).

aside from the bow of NS 12 is more intensive than that of NS 05, although the strength of the vorticity of NS 12 is less intensive at center plane. Due to the viscosity of fluid, the vorticity is diffused. On the other hand, even a slight vorticity can form an intensive vortex because of the stretching of vortex tubes, which is mainly caused by a local flow acceleration. The local flow acceleration of NS 12 is larger than that of NS 05 around the side of the bow. This situation is clearly observed at a higher Reynolds number flow in Fig. 9. This result is simillar with the result by Mori[7] who explained that the necklace vortex of the bow with a

NII-Electronic Library Service

The Society of Naval Architects of Japan

smaller curvature (circular cylinder) was more intensive than that of the bow with a larger one (elliptic strut) although the flow on the free surface around the bow of the elliptic strut was more unstable than that of the circular cylinder as mentioned before.

It can be concluded that the bow shape has strong relationship with the free surface curvature and this curvature, especially concave shape, is one of the sources of the vortical flows around the bow.

Fig. 10 shows the effect of Froude number for NS 05

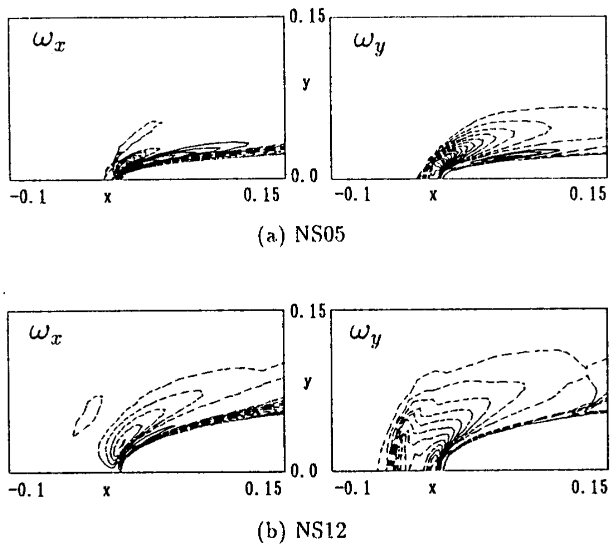

Fig. 9 Same as Fig. 8; Rn=10000, Fn=0.30, T=15.0 (contour interval=5.0).

at Rn=5000. Increasing Froude number, the vortical flows become more intensive and the gradient of the wave profile in front of the bow becomes steep. Strong reverse flow appears at a higher Froude number flow (Fn=0.35) around the juncture of the free surface and the strut. It can be expected that these vortical motions may become more intensive at a much higher Froude number flow and eventually the motions may make the flow unstable.

Fig. 11 shows the effect of the dynamic free surface boundary condition. In case of the zero-gradient extrapolation, the computed wave height at the bow is almost the same value as the position head at a stagnation point for inviscid fluid. On the other hand, the introduction of the no-shearing stress condition makes the counter-clockwise vorticity more intensive and the wave height decreases. This means that the energy accumulated around the wave crest is consumed by the generation of the vorticity. In case of a lower Froude number flow (Fn=0.25), however, there are no significant difference between the results as seen in Fig. 12.

It can be pointed out that the no-shearing stress condition on the free surface plays an important role to generate the vortical motions in case that the free surface curvature is large.

4.3 Grid dependence

Grid dependence on the vortical motions is investigated for NS 12 at Rn=5000 and Fn=0.30. Fig. 13 shows the effect of grid density in the vertical direction around the free surface; minimum grid spacings ($\Delta\zeta$) are 0.000

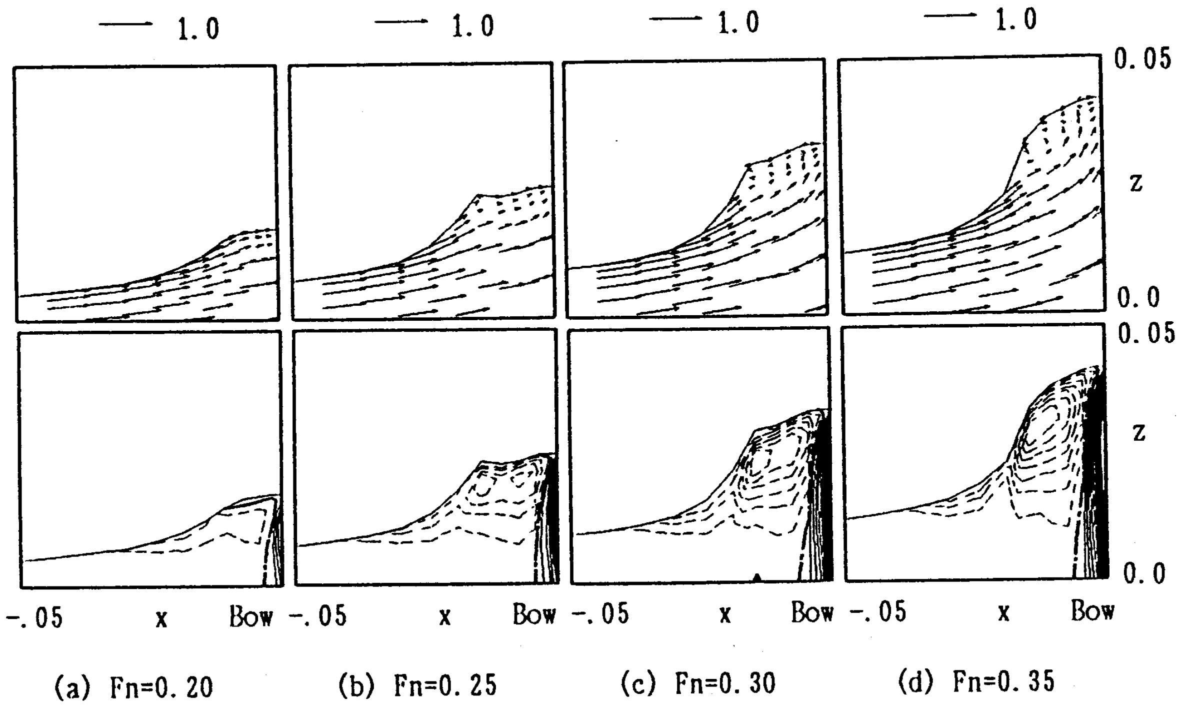

Fig. 10 Same as Fig. 6: effect of Froude number; NS05, Rn=5000, T=15.0 (contour interval=10.0)

NII-Electronic Library Service

The Society of Naval Architects of Japan

75, 0.0015 and 0.003 respectively. In case that $\Delta\zeta$ equals to 0.003, the vortical motions do not fully develop. On the other hand, the vortical motions develop well for other two cases and almost the same results are obtained for these two cases. Fig. 14 shows the grid dependence in the normal direction to the body surface. The total grid numbers are $91\times20\times20$, $91\times45\times20$ and $91\times65\times20$ respectively in the same computational domain as mentioned before. The minimum grid spacing in the normal direction to the body surface and the grid density in the vertical direction are the same for all the cases ($\Delta\zeta=0.0015$ and $\Delta\eta=0.002$). These results show that the grid density have a strong influence on the vortical motions; the coarse grid can not detect the vortical motions well.

4.4 Comparison with experiment

To validate the present computations, an experiment was carried out for the NS 12 model at the circulating water channel of Hiroshima University. The length and draft of the strut are 0.15m and 0.50m respectively. Wave profiles on the body surface were measured by use of an image processing system developed at Hiroshima University[12]. To remove the surface tension, a surfactant was used[13].

Fig. 15 shows the comparison between the computed and measured wave profiles on the body surface. The computed results give good agreement with the experi-

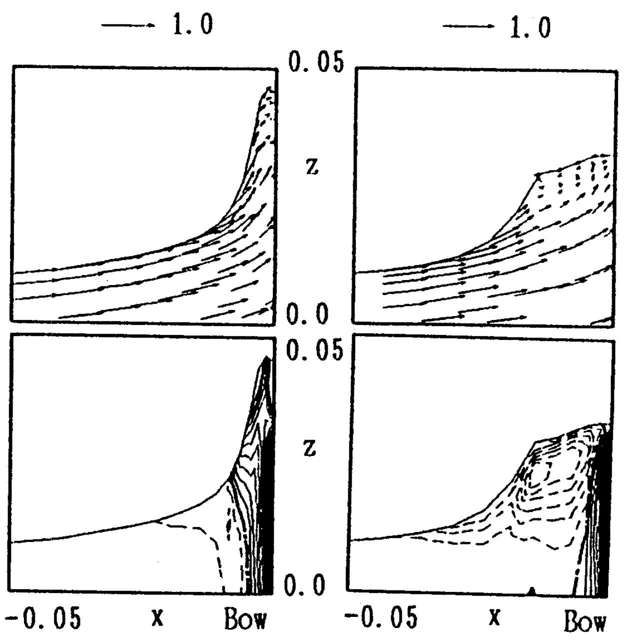

(a) zero-gradient (b) no-shearing stress

Fig. 11 Same as Fig. 6: effect of dynamic free surface boundary condition; NS05, Rn=5000, Fn=0.30, T=15.0 (contour interval =10.0).

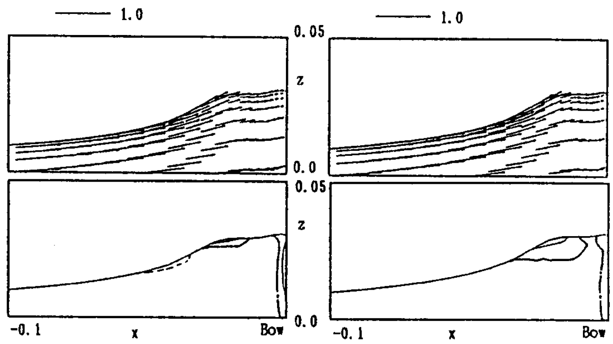

(a) no-shearing stress (b) zero-gradient

Fig. 12 Same as Fig. 6: effect of dynamic free surface boundary condition; NS12, Rn=5000, Fn=0.25, T=15.0 (contour interval=10.0).

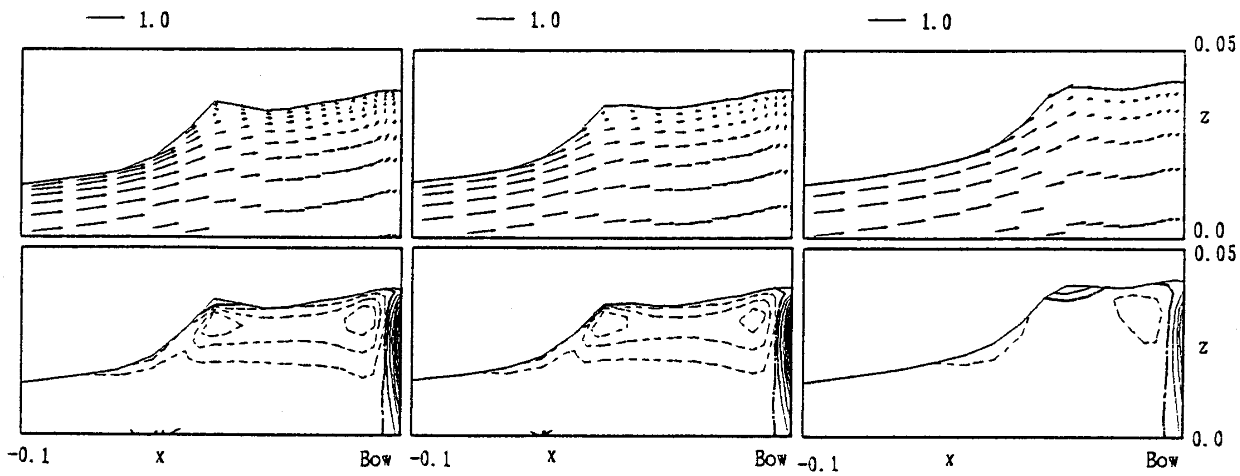

(a) $\Delta\zeta=0.00075$ (b) $\Delta\zeta=0.0015$ (c) $\Delta\zeta=0.0030$

Fig. 13 Same as Fig. 6: effect of grid density in vertical direction; NS12, Rn = 5000, Fn = 0.3, T = 15.0 (contour interval=10.0)

NII-Electronic Library Service

The Society of Naval Architects of Japan

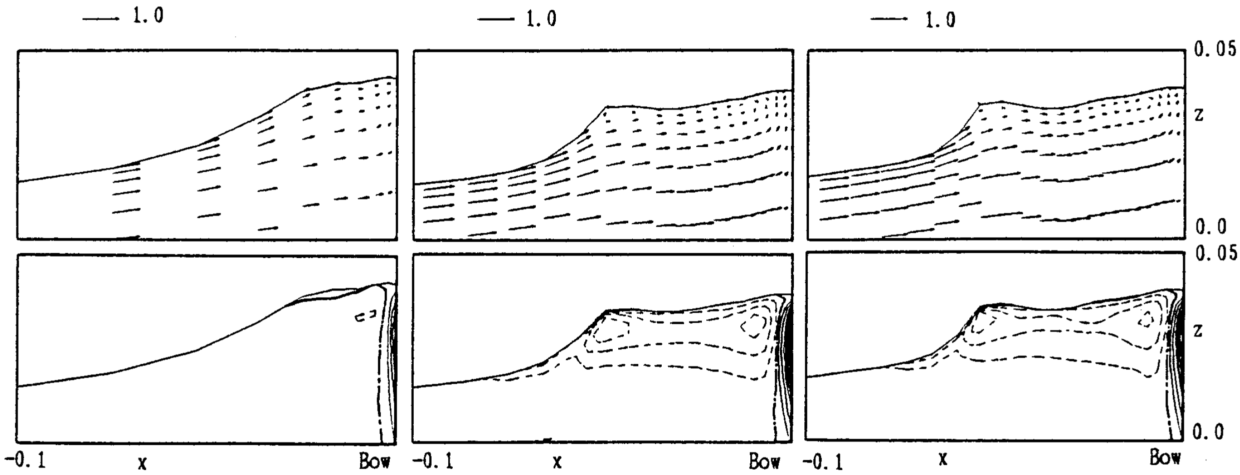

(a) 91 x 20 x 20 grid. (b) 91 x 45 x 20 grid. (c) 91 x 65 x 20 grid.

Fig. 14 Same as Fig. 6 : effect of grid density in normal direction to the body surface ; NS12, Rn = 5000, Fn = 0.3, T = 15.0 (contour interval = 10.0).

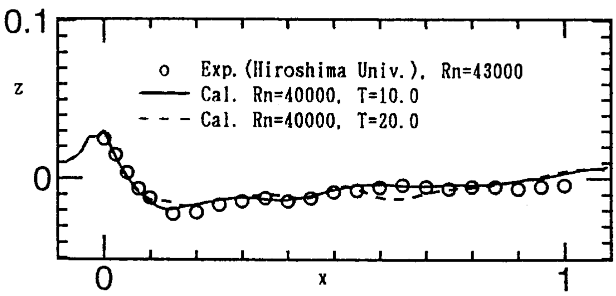

Fig. 15 Comparison between computed and measured wave profiles on the body surface ; NS12, Fn = 0.25.

mental one except near the wave trough. The reason of this difference may be that the flow around shoulder part of the blunt model is complicated including strong bubbly wake flow called shoulder wave breaking[14]. To detect this complicated flow, much finer grid must be used with some special treatment on the free surface such as a free surface turbulent model.

5. Concluding Remarks

Some characteristics of the vortical motions on the free surface are numerically investigated. Three different struts are used to investigate the curvature effect of the bow.

Findings through the present study are summarized as follows ;

1) In front of bow, the vorticity is generated to satisfy the no-shearing stress condition on the free surface and the vorticity induces the vortical motions beneath the free surface when the free surface curvature is large.

2) The bow with a larger curvature intensifies the concave curvature of the free surface and generates stronger vorticity than the bows with smaller curvature.

3) Grid density around the free surface is one of the important computational parameters ; coarse grid can not detect the vortical flows beneath the free surface.

The authors express their appreciation to Prof. K. Mori at Hiroshima University for his variable discussions and thanks are extended to Dr. S. Ninomiya, research associate at Hiroshima University, for his help for the experiments.

References

1) Baba, E. : *A New Component of Viscous Resistance of Ship, Journal of the Society of Naval Architects of Japan,* Vol. 125, (1969), pp. 23-34.
2) Taneda, S. and Amamoto, H. : *The Necklace Vortex of the Ship, Bulletin of Research Institude for Applied Mechanics,* Kyushu Univ., No. 31, (1969), pp. 17-28 (in Japanese).
3) Kayo, Y. and Takekuma, K. : *On the Free Surface Shear Flow related to Bow Wave-Breaking of Full Ship Models, Journal of the Society of Naval Architects of Japan,* Vol. 149, (1981), pp. 11-20.
4) Takekuma, K. and Eggers, K. : *Effect of Bow Shape on Free Surface Shear Flow, Proceedings of 15 th Symposium on Naval Hydrodynamics, Hamburg, Germany* (1984), pp. 387-405.
5) Ogiwara, S. et al. : *Experimental Investigation on Free Surface Flow Related to Bow Wave Breaking, Journal of the Kansai Society of Naval Architects of Japan, Vol.* 194, (1984), pp. 119-131 (in Japanese).
6) Miyata, H. et al. : *Numerical and Experimental Analysis of Nonlinear Bow and Stern Waves of a*

NII-Electronic Library Service

The Society of Naval Architects of Japan

Two-Dimensional Body (3 *rd Report*), *Journal of the Society of Naval Architects of Japan*, Vol. 156, (1984), pp. 1-12.

7) Mori, K.: *Necklace Vortex and Bow Wave around Blunt Bodies, Proceedings of 15 th Symposium on Naval Hydrodynamics, Hamburg, Germany* (1984), pp. 303-317.

8) Matsui, M. et al.: *Observation of Nonlinear Waves around Ship Bow Models, Journal of the Kansai Society of Naval Architects of Japan*, No. 190, (1983), pp. 63-71. (in Japanese)

9) Kodama, Y.: *Three Dimensional Grid Generation around a Ship Hull Using the Geometrical Method, Journal of the Society of Naval Architects of Japan*, Vol. 164, (1988), pp. 1-8.

10) Batchelor, G. K.: *An Introduction to Fluid Dynamics, Cambridge University Press*, (1970), pp. 364-366.

11) Hinatsu, M.: *Numerical Simulation of Unsteady Viscous Nonlinear Waves Using Moving Grid System Fitted on a Free Surface, Journal of the Kansai Society of Naval Architects of Japan*, No. 217, (1992), pp. 1-11.

12) Ninomiya, S., Mori, K., Hosokawa, M.: *Measurements of Wave Height by Visualizing Air-Side Free-Surface and Illuminating the Wetted Surface of Hull through Water, Journal of the Society of Naval Architects of Japan*, Vol. 174, (1993), pp. 129-135 (in Japanese).

13) Maruo, H. and Ikehata, H.: *Some Discussions on the Free Surface Flow around the Bow, Proceedings of 16 th Symposium on Naval Hydrodynamics, Berkeley, USA*, (1986), pp. 65-77.

14) Pogozelski, E., Katz, J., Huang, T.: *Flow Structure around a Surface-Piercing Blunt Body, Proceedings of 20 th Symposium on Naval Hydrodynamics, Santa Barbara, USA*, (1994), pp. 117 A-117 G.

NII-Electronic Library Service